DESIGN AND APPLICATION OF NANOCOMPOSITE BASED ON CLAY MINERAL (GLAUCONITE) AS ECO-FRIENDLY FERTILISER FOR AGRICULTURE

Maxim Rudmin [1,2], Boris Makarov [1], Prokopiy Maximov[1], Evan Dasi[1]

•

[1] Tomsk Polytechnic University, Russia
[2] University of Tyumen, Russia
rudminma@tpu.ru

Abstract

The application of nanocomposite fertilisers represents a progressive stride towards harmonising agronomical techniques with environmental conservation. Many studies have been embarked upon to gauge the effectiveness of fertilisers, engaging various substances encompassing polymers, clay minerals, and an amalgamation of synthetic and natural elements. Among these, using clay minerals, such as glauconite, which are both economical and readily accessible, provides an attractive substitute for numerous artificial substances. Glauconite is an adept inhibitor, consisting of nano and micro-particles with vast specific surface areas that maintain surface charge and provide ion-available interlayer sites, thus facilitating nutrient interchange.

This study explores constructing and using nanocomposite fertilisers from glauconite amalgamated with a carbamide solution-gel. The ensuing nanocomposite exhibits enhanced intercalation between ammonium and glauconite, as substantiated by extensive analyses using techniques such as XRD, TEM, FTIR, TG-DSC, SEM-EDS, Brunauer–Emmett–Teller (BET) analysis, soil leaching experiments, lab and field agricultural tests.

The mineral nanocomposites, replete with an assortment of novel functionalities, disclose that 20% of the carbamide solution results in an escalation of the intercalated N ratio to 8, predominantly within the smectite layers of glauconite. The decrease of a specific surface, the total pore volume and the average pore size in the nanocomposite reflects the adsorption of carbamide substances within the meso- and macropores of glauconite particles.

The chemically synthesised glauconite nanocomposite retains an original spherical morphology, accompanied by a distinctive microlayer near the surface, and exhibits an increased nitrogen ratio, indicative of a superior filtration capability. Controlled-action nitrogen and potassium nanocomposite fertiliser were realised using glauconite as an inhibitor.

The expectation of targeted and controlled release of nutrients such as ammonium, nitrate and potassium is facilitated by their multifarious forms within the glauconite. Chemically tailored glauconite nanocomposite confers numerous benefits, including a micro-granular mineral structure, a permeable internal morphology, the encapsulation of N compounds within diverse pore structures, and accessible potassium. Such characteristics of the nanocomposite aid in invigorating plant growth and development when these fertilisers are dispensed onto the soil.

Keywords: nanocomposites, glauconite, agriculture, fertilisers, intercalation, environmental conservation

I. Introduction

The agriculture is leaning towards controlled-release fertilisers (CRFs) for heightened efficiency and a safer environment [1–3]. Such fertilisers gradually deliver nutrients to plants,

reducing nutrient wastage and excessive accumulation in the soil, surface water, and groundwater [4–8]. Traditional fertilisers, including urea, ammonium nitrate, and ammonium sulfate, frequently lead to nitrogen build-up in agricultural land [9]. This surplus nitrogen can cause environmental damage through processes like denitrification and eutrophication of water bodies, contributing to greenhouse effects [10–13]. CRFs, therefore, aim not only to reduce these environmental hazards but also to bolster crop yield and quality [14–17]. Addressing the global challenge of feeding an ever-growing population necessitates such advancements [18,19].

Technologies underpinning CRFs can be grouped into chemical [7,20,21], mechanical [22–26] and mechanochemical [27–36] methods. Central to CRFs are inhibitory substances or containers ensuring targeted nutrient delivery to plants [37]. These inhibitors can be either polymeric substances [38,39], organo-polymeric compounds [40–44], or specific minerals [31,45–48]. Particularly noteworthy among these minerals are layered silicates like smectites [22,33,49,50], kaolinite [27,28,51], vermiculite [29,52], and glauconite [21,32,53,54].

Glauconite has drawn significant attention in the agricultural sector due to its inherent potassium-rich nature, making it a stand-alone mineral fertiliser [55–57]. It belongs to the dioctahedral potassium-rich iron-loaded phyllosilicate group within the 2:1 interlayer deficient mica family [58–62]. Historically, soils with glauconite have been linked to enhanced fertility [63]. This fertility boost was later attributed to the ion exchange capacity of glauconite, its moisture retention, and its naturally granulated form [21,55,64,65]. Intriguingly, glauconite often contains smectite layers, the proportion of which depends on the mineral's maturity. While the absorption capacity of smectite has been extensively studied, glauconite's potential still needs to be explored. However, recent research has demonstrated nitrogen intercalation with glauconite, which culminates in superior fertilisers promoting enhanced plant growth [32,53,54].

This research delves deep into the interaction between globular glauconite and carbamide solution, targeting the intercalation of nitrogen compounds to produce high-quality nanocomposite fertiliser. The study features experiments on applying glauconite-carbamide nanocomposite fertilisers in different plant growth tests.

II. Methods

The nanocomposite was formulated using glauconite and a solution of carbamide. Glauconite from the Karin deposit in Russia was utilized in this research [21]. Energy dispersive X-ray spectroscopy analysis reveals the original chemical makeup of glauconite to include the following components: 6.8-9.4 wt.% K_2O, 18.1-32.9 wt.% $Fe_2O_{3(total)}$, 50.2-58.2 wt.% SiO_2, 3.8-11.8 wt.% Al_2O_3, 2.9-4.7 wt.% MgO, 0.4-0.6 wt.% CaO, 0.3-0.4 wt.% Na_2O and 1.7-4.5 wt.% LOI (loss on ignition). The crystal-chemical formula is: $K_{0.6\text{-}0.8}(Al_{0\text{-}0.7}Mg_{0.3\text{-}0.5}Fe_{0.9\text{-}1.7})_{1.6\text{-}2.0}(Si_{3.5\text{-}3.8}Al_{0.2\text{-}0.6})O_{10}(OH)_2nH_2O$. X-ray diffraction patterns of oriented glauconite samples indicate the amount of the expanded smectite layers around 8%. The carbamide (CH_4N_2O) solution gel, provided by Terra Master Ltd. in Russia, contains in excess of 25% of nitrogen.

The chemical activation process for the nanocomposite was conducted with naturally granulated glauconite concentrate over 48 hours. A 4:1 glauconite to nitrogen (N concentration in carbamide solution) ratio was adopted, guided by prior experience. The final product of this process was given the name Gk4N1.

The characteristics of the crafted nanocomposites were studied using an array of methods [21]. This included X-ray diffraction (XRD), scanning electron microscopy with energy dispersive X-ray spectroscopy (SEM-EDS), transmission electron microscopy (TEM) with selected area electron diffraction (SAED), Fourier transform infrared spectroscopy (FTIR), and differential thermal analysis (incorporating thermo-gravimetric analysis and differential scanning calorimetry, TG-DSC), alongside a quadrupole mass spectrometer and Brunauer–Emmett–Teller (BET) analysis.

Examinations of the structural alterations in glauconite occurred before and after nanocomposites' activation. The mineral composition of randomly arranged nanocomposites was discerned using a Bruker D2 Phase X-ray diffractometer with specific settings. This included taking scans of composite fractions under specific conditions, separating the clay fraction and preparing them with various techniques for further analysis. Each sample was measured in the air-dried and the ethylene-glycol solvated states following placement in a desiccator for 24 h at ~60 °C.

The unit structures and interlayers of glauconite crystals were explored at the Center for Sharing Use "Nanomaterials and Nanotechnologies" of Tomsk Polytechnic University through JEOL JEM-2100F transmission electron microscopy (TEM). The images were explicitly captured using a copper grid and certain technical details.

FTIR spectra were gathered using a specific spectrometer to identify the chemical bond functional groups within the nanocomposites. The temperature-controlled high-sensitivity detector was used to obtain data between specific wave numbers.

TG-DSC curves were taken to study thermal degradation and calculate the weight ratio of different intercalations using a specific micro thermal analyser under an inert argon atmosphere.

The analysis was coupled with a mass spectrometer for simultaneous detection and quantification of evolved gases, with calibration performed before the experimentation and certain additional adjustments made.

The nanocomposites underwent analysis under a TESCAN VEGA 3 SBU scanning electron microscope, operating with specific technical parameters, followed by elemental analysis through an OXFORD X-Max 50 energy-dispersive adapter.

The BET method was employed to evaluate the specific surface of the samples using a particular adsorption-specific surface and porosity analyser, with specific drying and degassing procedures followed.

For the leaching experiment, dry sandy soil was combined with nanocomposites, and specific dosing and procedures were applied. A PVC tube was utilized, and specific modifications were made to collect leachate. The trial was replicated three times, and specific methods were employed to maintain the soil moisture level and monitor various concentrations. The final values were computed as an average, and additional calculations were performed for cumulative release curves.

Statistical examination of the outcomes was carried out with Microsoft Excel 365, with values computed as arithmetic means alongside standard deviations. Statistical tests were performed to ascertain significant variances between the experiments, including the least significant difference (LSD) test at the 0.05 probability level, following analyses of variance, which the LSD then followed.

Agrochemical experiments were carried out in laboratory and field conditions.

Experiments were conducted in the laboratory to cultivate agricultural crops, explicitly utilising promising nanocomposites. Soil devoid of fertilisers served as a control and standardisation plot. Oat seeds (*Avéna satíva*) were grown at a consistent room temperature (26±1 °C) for a duration of 20 days within glass Petri dishes, each having dimensions of 9 cm in diameter and 1.5 cm in depth.

Both dry composite products and urea were incorporated into the soil at a rate of 50 kg (potassium) per hectare. The experiment was replicated on three occasions (one plot), and the mean values were subsequently recorded.

A weakly acidic dark grey agricultural soil (pH 5.1) containing 4.1% organic carbon was employed for these trials. The plants were consistently watered using tap water each morning. Standard methods were used to determine the plants' germination energy, height, and dry weight (yield).

Germination was gauged by calculating the proportion of sprouts to the overall number of seeds

planted. Germination energy was monitored daily, and the final germination percentage was ascertained after four days. The number of sprouts was deduced, assuming the plants reached 2 cm above the soil surface.

Following the 20-day period, measurements were taken of the plant's height and weight. The oat seedlings were individually enclosed in paper sheets and preserved in a desiccator at 80 °C. Once the weight of the plant samples had stabilised, their dry weight (yield) was measured.

The nanocomposite was specifically trialled on wheat in field-based growth experiments concerning plant cultivation. The fertiliser was applied at a rate of 90 kg per hectare, with the overall experimental plot encompassing an area of 0.25 hectares. The structure of the wheat yield (crop yield, plant height, ear count) was ascertained from a selected 1 square meter area, where 30 plants were chosen from the collective sheaf. The yield was quantified based on the weight of the threshed crop and subsequently translated into kg per hectare.

To assess the quality of the wheat, parameters such as moisture content, protein content, and gluten composition were analysed. This analysis used an NIR-analyser, specifically the "Infralum FT 10" model (Lumex, Russia). The process entailed conducting three individual measurements, the mean of which was then computed to accurately represent the aforementioned indicators.

III. Results

The X-ray diffraction pattern of the activated nanocomposite (Fig. 1) displays characteristic peaks of glauconite, carbamide (urea), and quartz impurity. Compared to the raw glauconite, the diffraction patterns of the activated nanocomposites reveal a new basal 001 peak, corresponding to the increased inter-planar space of the expanding smectite layers in glauconite at 17.0 Å. The occupation of the interplanar distance by new ions is confirmed by the absence of displacement of this basal peak in the ethylene–glycol solvated state of the nanocomposite (Fig. 1). The diffraction pattern is marked by peaks at 4.0, 3.6, 3.2, 3.0, and 2.5 Å, which are associated with adsorbed urea. The glauconite's characteristic peaks occur at 10.0, 4.5, 2.6, and 2.45 Å.

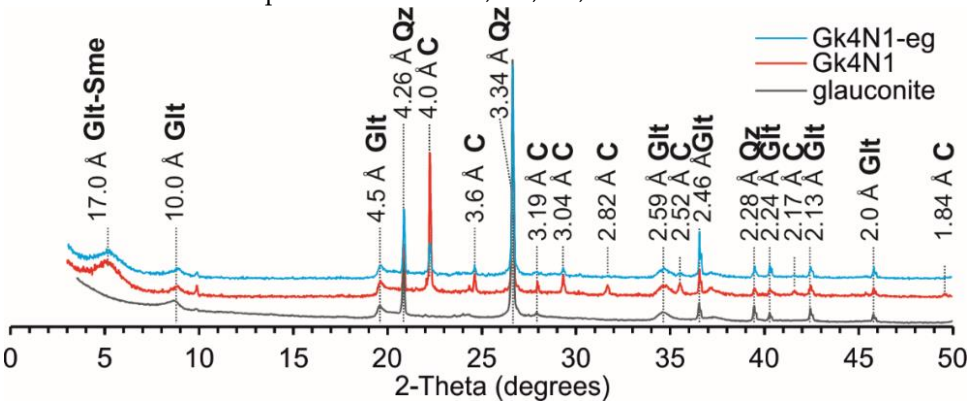

Fig. 1: *X-ray patterns for both the activated nanocomposite and the glauconite. The sample labelled Gk4N1-eg represents the nanocomposite scanned in its ethylene–glycol solvated state. C – carbamide, Glt – glauconite, Glt-Sme – glauconite-smectite, Qz – quartz*

High-resolution images and local electron diffraction patterns showcase nanocomposite particles of glauconite with expanded crystal bundles. Nanocomposite particles often display an augmentation of single or double mineral unit structures. The typical interlayer thickness in the native glauconite varies from 1.9-2.7 nm but is notably thicker in the nanocomposite 2.8-3.9 nm.
The IR spectrum of the nanocomposite (Fig. 2) displays variations at 1155, 1452-1462, 1600, 1624, 1680, 3342, and 3442 1/cm. The nanocomposite retains certain glauconite-specific vibrations at 700, 775, 794, and 1020 1/cm in tetrahedral positions, $Fe^{II}OHFe^{III}$ and $MgOHFe^{III}$ in octahedral positions

at 3522 and 3564 1/cm, respectively [58,66]. During activation with glauconite, the intensities of certain NH_2 at 1155 and 3442 1/cm and NH peaks at 1680 and 3342 1/cm become more pronounced. A distinct peak in the nanocomposite is linked to the CO vibrations of the adsorbed urea at 1600 1/cm.

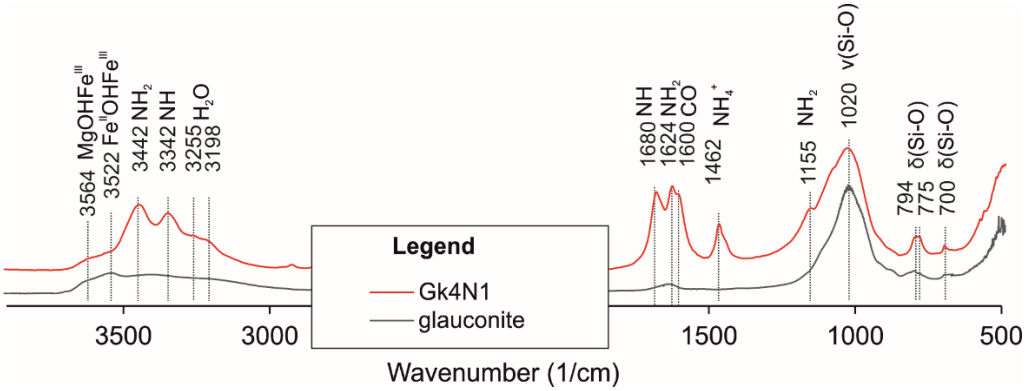

Fig. 2: *FTIR spectra of the nanocomposite and the original glauconite*

The nanocomposite DSC curve (Fig. 3 A) indicates two pronounced endothermic effects and one subtle endothermic effect at 134°C, 188°C, and 360°C, respectively. Furthermore, there are four exothermic responses at 122°C, 153°C, 290°C, and 650°C. The initial sharp endothermic response at 134°C signifies the melting of carbamide. The subsequent endothermic change, occurring between 184-190°C, corresponds to the evaporation of carbamide — specifically NH3 and CO2. This is associated with the components integrated into the mineral. The milder endothermic reaction at 360°C confirms the breakdown of the polymerised component of carbamide. Notably, an endothermic effect at 571°C indicates a minor presence of quartz.

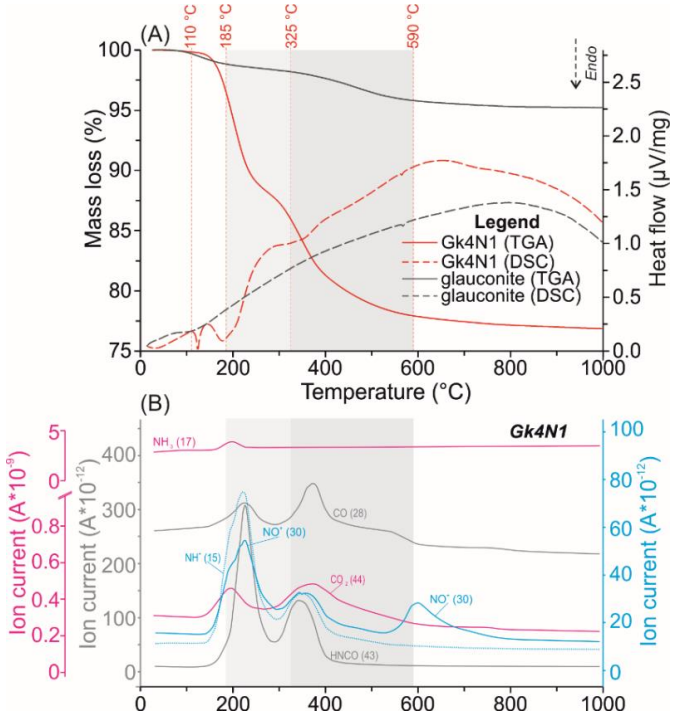

Fig. 3: *(A) TGA (represented by solid lines) with DSC curves (indicated by dashed lines) of the prepared nanocomposite and the original glauconite. (B) Highlighted representative MS ion detection curves with m/z values of 15 (NH^+), 17 (NH_3), 28 (CO^+), 30 (NO^+), 43 ($HNCO^+$), and 44 (CO_2).*

The TG curve of the nanocomposite (Fig. 3 A) outlines five primary weight loss phases that

are indicative of glauconite: spanning temperature ranges of 0-110°C, 110-185°C, 185-325°C, 325-590°C, and 590-1000°C. The initial phase (0-110°C) is attributed to eliminating physically attached water from the mineral, resulting in a 0.1-0.2 wt.% weight loss. The subsequent phase (110-185°C) pertains to the expulsion of water and carbamide by-products (NH_3 and CO_2) from the nanocomposite's macropore space (Fig. 3 B), resulting in weight reductions of 0.7-3.3 wt.%. The third phase (185-325°C) encompasses the release of mesopore water and several carbamide breakdown products. The weight decrease within this span is 2.1-10.6 wt.%. The fourth weight loss phase, 325-590°C, sees nanocomposite weight loss ranging from 2.5 to 8.0 wt.%. This stage is linked to expulsing water and carbamide degradation products, predominantly from the mineral interlayer space. Additionally, an elevated concentration of carbamide in the nanocomposites is evident from the observed releases of CO_2, CO, HNCO, NO^+, and NH^+. The final phase, between 590-1000°C, results in a 0.6-1.1 wt.% weight loss, reflecting the dehydration of the glauconite crystal structures within the nanocomposite.

Both the nanocomposite and the original glauconite exhibit a globular grain size, with lengths varying between 50 and 250 μm (Fig. 4). Haphazardly oriented micro-flakes with sinuous borders characterise the internal morphology of these globules. These micro-flakes range in size from 0.5-5 μm in length. One distinguishing feature of the glauconite near-surface microlayer is the parallel alignment of micro-flakes perpendicular to the surface. Furthermore, these nanocomposite microlayers are marked by a higher nitrogen content than the globules core.

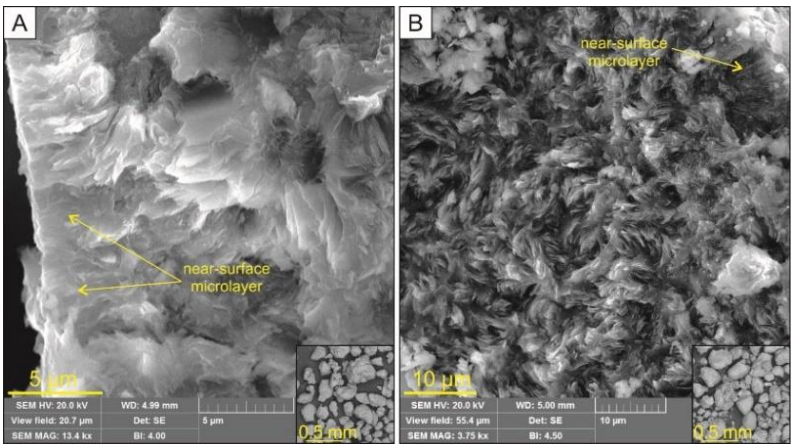

Fig. 4: *SEM photos captured using a secondary electron detector showcasing the distinct morphological characteristics of the nanocomposite (A) as opposed to the original glauconite (B). The bottom right corner provides an encompassing image of the globular section for each sample.*

The original globular glauconite specific surface area, pore volume, and average pore size are 41.2 m^2/g, 0.064 cm^3/g, and 8.9 nm, respectively. As the proportion of carbamide increases during activation, the specific surface area of the nanocomposite drops to 23.8 m^2/g. In tandem, the average pore volume and size reduce to 0.036 cm^3/g and 4.1 nm, respectively.

The laboratory soil leaching examinations provided varied insights into the leaching kinetics of ammonium, nitrate, and potassium from the nanocomposite. For ammonium (Fig. 5 A), two prominent release phases were observed: days 1-7 and 21-28. Between days 7 and 21, the release of ammonium was gradual. After the 28th day, the release rate became more measured and extended. In contrast, nitrates exhibited a notably rapid release within seven days (Fig. 5 B). Beyond this, only trace amounts, ranging from 0.2 to 0.3 mg, were leached from day 7 to day 56. The leaching kinetics of potassium from the nanocomposites (Fig. 5 C) progressed through four distinct phases, setting them apart from the potassium leaching kinetics observed in the control sample. The first phase, lasting until day 7, saw a rapid release. This was followed by a period of slower release from day 7 to day 28. The period from day 28 to day 43 marked the peak release

rate.

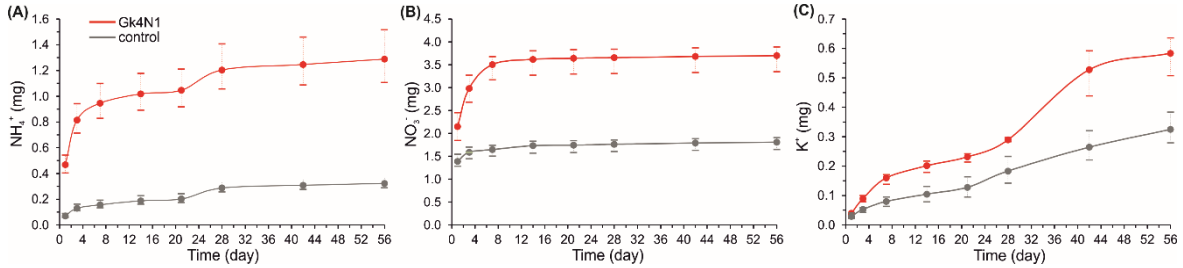

Fig. 5: *Cumulative graphs detailing the release rates of ammonium (A), nitrate (B), and potassium (C) from the nanocomposite. These are set against a control sample devoid of nanocomposite from laboratory assessments. The dotted lines depict the range between the minimum and maximum cumulative values. Any statistically significant variances for each parameter are noted at the p = 0.05. Error bars denote standard deviations.*

The dry weight of the oat (*Avéna satíva*) exhibited an increase in the laboratory plant growth experiment when the tested nanocomposite was used, compared to the control (Fig. 6). The recorded dry weight (or crop yield) stood at 0.266 g, which is in contrast to the 0.233 g for the control sample (Fig. 6 A). This indicates a boost in crop yield by over 14.2% in the plots treated with the nanocomposite. Regarding the germination rate (Fig. 6 B), the presence of the nanocomposite led to an increase of 93.3%, whereas the control plot (without any fertiliser) recorded a rate of 90.7%. As for the average plant height (Fig. 6 C), there was a rise to 14.3 cm in the nanocomposite-treated plot, in contrast to the control's 12.7 cm. This denoted an elevation in plant height by 12.6% when the devised nanocomposite was applied.

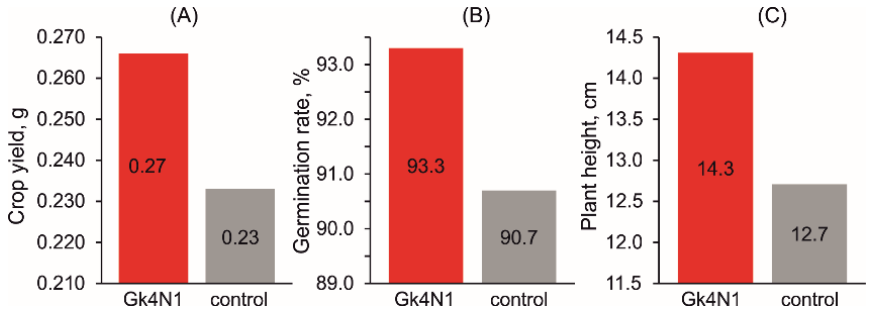

Fig. 6: *Yield (A), germination rate (B), and plant height (D) of oat (Avéna satíva) were assessed following the application of the researched nanocomposite fertilisers and compared to a control plot without any fertilisers, based on laboratory experiments. Each parameter's statistical significance is highlighted at the p = 0.05 level.*

Field agro experiment with wheat cultivation also showed the stimulating effect of nanocomposite as a fertiliser on yield. The experiment yield with nanocomposite was 5.7 t/ha compared to 4.5 t/ha in the control plot. This indicates a 27.4% increase in wheat yield. The structure and quality of wheat also differed in the experiments with nanocomposite relative to the control (Table 1). An increase in all the wheat structure indices (average ear length and ear count) was recorded. The average plant height and ear count changed from 8.5 to 9.1 cm and 36 to 42 pieces, respectively, relative to the control. These indicators increase by 7.5 and 16.9%. Moisture, protein and gluten content vary relative to the control from 16 to 16.4%, 11.3 to 13.2% and 10.6 to 19%, respectively.

Table 1: *Wheat yield average indicators based on the results of field experiments*

	Crop yield, t/ha	Spike length, cm	Average ear count	Moisture content, %	Protein content, %	Gluten composition, %
Nanocomposite	4.5	8.5	36	16.0	11.3	10.6
Control	5.7	9.1	42	16.4	13.2	19.0

IV. Discussion

In the activated nanocomposite, the proportion of intercalated nitrogen mixtures is ascertained by the initial basal XRD reflex shift to 17.0 Å (Fig. 1), the linear measurements of the expansion in inter-planar distance captured on TEM images, and the weight reduction between temperatures of 325-590 °C. This is further corroborated by the release of nitrogen compounds revealed by TG-DSC-MS data (Fig. y). As nitrogen concentration in the resultant solution rises, correlating to a 20 mol.% of the glauconite concentrate, the intercalated nutrient ratio also surges to a peak of 8.0%. Interestingly, this maximal intercalation does not surpass the proportion of smectite layers present in glauconite. This reflects the specific intercalation capacity of the inter-planar gaps within the smectite phases [21,53,54,67]. This might be due to the ionic exchange involving ammonium and solvate water and the sodium and calcium native to the mineral.

Consequently, calcium and sodium are scarcely present in the nanocomposites, while the primary elements (Si, Al, Fe, Mg, K) remain consistent with the original mineral's proportions. Therefore, the intercalation aptitude of glauconite seems reliant on the number of its smectite layers, its [62] or maturity [60], and the geological conditions [68,69].

Using FTIR peaks (Fig. 2), adsorbed nitrogen compounds in meso- and macropores are determined by NH2 and NH signatures. These are further indicated by weight losses between 100-185 °C (macropores) and 185-325 °C (mesopores), revealing the presence of specific ions (Fig. 3). The subsequent decline in total pore volume and mean pore diameter authenticates the filling of meso- and macro-pores.

An evident microlayer on the surface of glauconite globules (Fig. 4), alongside oriented micro-flakes, underscores the mineral's advantageous morphological attributes. A heightened nitrogen presence within these microlayers suggests a superior filtration capability. It's theorised that carbamide penetrates glauconite globules mainly via these solution-conducting microlayers and subsequently permeates the core. Within the core, nitrogen compounds are intercalated between the smectite layers of glauconite and are also absorbed in mesopore spaces.

Nutrient releases, encompassing ammonium, nitrate, and potassium, reveal a stepwise kinetics aligned with their interaction with the mineral (Fig. 5). The initial, easily accessible forms relate to substances adsorbed in macropores, and they're typically discharged from the nanocomposites within the initial 21 days or 7 days for ammonium and nitrate, respectively. This is followed by releasing absorbed ammonium from the mesopore region from day 21 to 28. By the 28th day, the intercalated ammonium is extracted from the mineral's interlayer. The staggered kinetics of these nutrient releases, particularly for ammonium and potassium, accentuates the dual positive role of layered glauconite in nanocomposites as both an ammonium suppressor and a potassium source.

The resultant mineral nanocomposites, crafted by chemically activating globular glauconite with carbamide, offer multiple benefits. They retain a micro-granular mineral form, possess an innate diffusive microlayer, incubate nitrogen elements across micro-, meso-, and macro-pores, and act as a potassium source. There's a specific interest in the ammonium intercalation within the smectite layers of these mineral constructs, underscoring the significance of understanding glauconite's structural integrity.

Laboratory and field tests revealed a pronounced positive effect on plant growth and

development without the risk of environmental damage when using a nanocomposite derived from the innate globular structure of glauconite (Fig. 6, Table 1). In controlled laboratory conditions, the assessed nanocomposite fertiliser consistently improved oat growth. Additionally, under field conditions, introducing the Gk4N1 nanocomposite into the soil remarkably boosted the quality and quantity of wheat yield – with an impressive 27.4% increase in yield. This significant growth surpasses the outcomes of applying unaltered glauconite in the field [65,70].

V. Conclusions

From the research into the chemical activation of globular glauconite with carbamide and the subsequent use of this nanocomposite, the following key findings have been established.

Within the interlayer spaces (micropores) of smectite layers in glauconite, nitrogen intercalation occurs. Utilising a carbamide solution with a 20% nitrogen concentration facilitates optimal intercalation.

The presence of adsorbed carbamide substances in meso- and macropores is indicated by a reduced specific surface area, total volume, and mean pore diameter in the nanocomposite.

Glauconite nanocomposites retain their globular particle shape and exhibit a unique near-surface microlayer. An elevated nitrogen concentration in these surface microlayers underscores their superior filtration capability. This surface microlayer plays a crucial role in delivering solutes to the core region of glauconite globules.

The nanocomposites show a staggered nutrient release mechanism, underlining the varied absorption of carbamide in the micro-, meso-, and macro-pores of glauconite. Moreover, alongside nitrogen compounds, potassium is also gradually released from the glauconite nanocomposites.

Introducing the nanocomposite into the soil as a fertiliser enhances both the quality and quantity of crop yields. Importantly, laboratory and field tests confirm this is achieved without posing environmental hazards.

The authors gratefully acknowledge the financial support provided by Russian Science Foundation through the research project № 22-77-10002.

References

[1] Duan, Q.; Jiang, S.; Chen, F.; Li, Z.; Ma, L.; Song, Y.; Yu, X.; Chen, Y.; Liu, H.; Yu, L. (2023). Fabrication, evaluation methodologies and models of slow-release fertilizers: A review. *Industrial Crops and Products*, 192:1–22.

[2] Sharma, G.C. (1979). Controlled-release fertilizers and horticultural applications. *Scientia Horticulturae*, 11:107–129.

[3] Trenkel, M.E. Controlled-Release and Stabilized Fertilizers in Agriculture, Paris, 1997.

[4] Trenkel, M.E. Slow- and Controlled-Release and Stabilized Fertilizers: An Option for Enhancing Nutrient Use Efficiency in Agriculture, Paris, 2010.

[5] Oertli, J.J. (1980). Controlled-release fertilizers. *Fertilizer Research*, 1:103–123.

[6] Ni, B.; Liu, M.; Lu¨, S.; Xie, L.; Wang, Y. (2011). Environmentally Friendly Slow-Release Nitrogen Fertilizer. *Journal of Agricultural and Food Chemistry*, 59:10169–10175.

[7] Chen, L.; Chen, X.L.; Zhou, C.H.; Yang, H.M.; Ji, S.F.; Tong, D.S.; Zhong, Z.K.; Yu, W.H.; Chu, M.Q. (2017). Environmental-friendly montmorillonite-biochar composites: Facile production and tunable adsorption-release of ammonium and phosphate. *Journal of Cleaner Production*, 156:648–659.

[8] Chakraborty, R.; Mukhopadhyay, A.; Paul, S.; Sarkar, S.; Mukhopadhyay, R.)2023). Nanocomposite-based smart fertilizers: A boon to agricultural and environmental sustainability.

Science of The Total Environment, 863:160859.

[9] Alrbaihat, M.R. (2023). Agricultural Nano Fertilizers: Macronutrient Types and Applications Review. *Current Trends in Geotechnical Engineering and Construction*, 306–316.

[10] Obieze, C.C.; Chikere, C.B.; Adeleke, R.; Akaranta, O. (2019). Formulation and evaluation of slow-release fertilizer from agricultural and industrial wastes for remediation of crude oil-polluted soils. *Society of Petroleum Engineers - SPE Nigeria Annual International Conference and Exhibition*, NAIC 2019.

[11] Akiyama, H.; Yan, X.; Yagi, K. (2010). Evaluation of effectiveness of enhanced-efficiency fertilizers as mitigation options for N_2O and NO emissions from agricultural soils: Meta-analysis. *Global Change Biology*, 16:1837–1846.

[12] Xiao, Y.; Peng, F.; Zhang, Y.; Wang, J.; Zhuge, Y.; Zhang, S.; Gao, H. (2019). Effect of bag-controlled release fertilizer on nitrogen loss, greenhouse gas emissions, and nitrogen applied amount in peach production. *Journal of Cleaner Production*, 234:258–274.

[13] IPCC Climate Change 2014: Mitigation of Climate Change: Working Group III Contribution to the Fifth Assessment Report of the Intergovernmental Panel on Climate Change 2014.

[14] Mala, R.; Selvaraj, R.; Sundaram, V.; Rajan, R.; Gurusamy, U. (2017). Evaluation of Nano Structured Slow Release Fertilizer on the Soil Fertility, Yield and Nutritional Profile of Vigna radiata. *Recent Patents on Nanotechnology*, 11:50–62.

[15] Liu, Q.; Liu, Y.; Hao, X.; Song, C.; Zong, Y.; Zhang, D.; Shi, X.; Li, P. (2023). Effects of controlled-release fertilizer on N_2O emissions in wheat under elevated CO2 concentration and temperature. *Plant and Soil*, 3:1–19.

[16] Pereira, E.I.; A. Nogueira, A.R.; Cruz, C.C.T.; Guimarães, G.G.F.; Foschini, M.M.; Bernardi, A.C.C.; Ribeiro, C. (2017). Controlled Urea Release Employing Nanocomposites Increases the Efficiency of Nitrogen Use by Forage. *ACS Sustainable Chemistry & Engineering*, 5:9993–10001.

[17] Fu, J.; Wang, C.; Chen, X.; Huang, Z.; Chen, D. (2018). Classification research and types of slow controlled release fertilizers (SRFs) used - a review. *Communications in Soil Science and Plant Analysis*, 49: 2219–2230.

[18] Pretty, J.; Sutherland, W.J.; Ashby, J.; Auburn, J.; Baulcombe, D.; Bell, M.; Bentley, J.; Bickersteth, S.; Brown, K.; Burke, J.; et al. (2010). The top 100 questions of importance to the future of global agriculture. *International Journal of Agricultural Sustainability*, 8:219–236.

[19] Tilman, D.; Cassman, K.G.; Matson, P.A.; Naylor, R.; Polasky, S. (2002). Agricultural sustainability and intensive production practices. *Nature*, 418:671–677.

[20] Rashid, M.; Hussain, Q.; Khan, K.S.; Alwabel, M.I.; Hayat, R.; Akmal, M.; Ijaz, S.S.; Alvi, S.; Obaid-ur-Rehman (2021). Carbon-Based Slow-Release Fertilizers for Efficient Nutrient Management: Synthesis, Applications, and Future Research Needs. *Journal of Soil Science and Plant Nutrition*, 1–26.

[21] Rudmin, M.; Maximov, P.; Dasi, E.; Kurovsky, A.; Gummer, Y.; Ibraeva, K.; Kutugin, V.; Soktoev, B.; Ponomarev, K.; Tararushkin, E.; et al. (2023). Intercalation of carbamide to globular glauconite by chemical processing for the creation of slow-release nanocomposites. *Applied Clay Science*, 243:107075.

[22] Rudmin, M.; Banerjee, S.; Makarov, B.; Ibraeva, K.; Konstantinov, A. (2022). Mechanical Activation of Smectite-Based Nanocomposites for Creation of Smart Fertilizers. *Applied Sciences*, 12:1–11.

[23] Singla, R.; Alex, T.C.; Kumar, R. (2020). On mechanical activation of glauconite: Physicochemical changes, alterations in cation exchange capacity and mechanisms. *Powder Technology*, 360:337–351.

[24] Salimi, M.; Motamedi, E.; Safari, M.; Motesharezedeh, B.; Motesharezadeh, B. (2021). Synthesis of urea slow-release fertilizer using a novel starch-g-poly(styrene-co-butylacrylate) nanocomposite latex and its impact on a model crop production in greenhouse. *Journal of Cleaner Production*, 322:129082.

[25] Zhao, X.; Qi, X.; Chen, Q.; Ao, X.; Guo, Y. (2020). Sulfur-Modified Coated Slow-Release

Fertilizer Based on Castor Oil: Synthesis and a Controlled-Release Model. *ACS Sustainable Chemistry & Engineering*, acssuschemeng.0c06056.

[26] Mañosa, J.; la Rosa, J.C.; Silvello, A.; Maldonado-Alameda, A.; Chimenos, J.M. (2023). Kaolinite structural modifications induced by mechanical activation. *Applied Clay Science*, 238:106918.

[27] Solihin; Zhang, Q.; Tongamp, W.; Saito, F. (2011). Mechanochemical synthesis of kaolin–KH2PO4 and kaolin–NH4H2PO4 complexes for application as slow release fertilizer. *Powder Technology*, 212: 354–358.

[28] Alrbaihat, M.R.; Al-Rawajfeh, A.E.; Alshamaileh, E. (2021). A mechanochemical preparation, properties and kinetic study of kaolin-N, P fertilizers for agricultural applications. *Journal of the Mechanical Behavior of Materials*, 30:265–271.

[29] De Oliveira, D.S.; Jaerger, S.; Marangoni, R. (2021). Mechanochemical Synthesis of Expanded Vermiculite with Urea for Filler into Alginate/Collagen Spherical Capsules: A Urea Slow-release System. *Orbital: The Electronic Journal of Chemistry*, 13:124–130.

[30] AlShamaileh, E.; Alrbaihat, M.; Moosa, I.; Abu-Afifeh, Q.; Al-Fayyad, H.; Hamadneh, I.; Al-Rawajfeh, A. (2022). Mechanochemical Preparation of a Novel Slow-Release Fertilizer Based on K2SO4-kaolinite. *Agronomy*, 12:3016.

[31] Borges, R.; Baika, L.M.; Grassi, M.T.; Wypych, F. (2018). Mechanochemical conversion of chrysotile/K2HPO4 mixtures into potential sustainable and environmentally friendly slow-release fertilizers. *Journal of Environmental Managemen*t, 206:962–970,.

[32] Rudmin, M.; Abdullayev, E.; Ruban, A.; Buyakov, A.; Soktoev, B. (2019). Mechanochemical Preparation of Slow Release Fertilizer Based on Glauconite–Urea Complexes. *Minerals*, 9:507.

[33] Borges, R.; Prevot, V.; Forano, C.; Wypych, F. (2017). Design and Kinetic Study of Sustainable Potential Slow-Release Fertilizer Obtained by Mechanochemical Activation of Clay Minerals and Potassium Monohydrogen Phosphate. *Industrial & Engineering Chemistry Research*, 56:708–716.

[34] Said, A.; Zhang, Q.; Qu, J.; Liu, Y.; Lei, Z.; Hu, H.; Xu, Z. (2018). Mechanochemical activation of phlogopite to directly produce slow-release potassium fertilizer. *Applied Clay Science*, 165:77–81.

[35] Borges, R.; Giroto, A.S.; Guimarães, G.G.F.; Reis, H.P.G.; Farinas, C.S.; Ribeiro, C. (2022). Asbestos cement waste treatment through mechanochemical process with KH2PO4 for its utilization in soil pH correction and nutrient delivery. *Environmental Science and Pollution Research*, 1:1–12.

[36] Alrbaihat, M.; AlShamaileh, E.; Al-Rawajfeh, E. (2022). Environment-Friendly Synthesis of Feldspar-KH2PO4 Complexes by Mechanochemical Reaction. BOHR International *Journal of Material Sciences and Engineering*, 1:1–6.

[37] Rahman, M.H.; Haque, K.M.S.; Khan, M.Z.H. (2021). A review on application of controlled released fertilizers influencing the sustainable agricultural production: A Cleaner production process. *Environmental Technology & Innovation*, 23:101697.

[38] Pereira, E.I.; da Cruz, C.C.T.; Solomon, A.; Le, A.; Cavigelli, M.A.; Ribeiro, C. (2015). Novel Slow-Release Nanocomposite Nitrogen Fertilizers: The Impact of Polymers on Nanocomposite Properties and Function. *Industrial & Engineering Chemistry Research*, 54:3717–3725.

[39] González, M.E.; Cea, M.; Medina, J.; González, A.; Diez, M.C.; Cartes, P.; Monreal, C.; Navia, R. (2015). Evaluation of biodegradable polymers as encapsulating agents for the development of a urea controlled-release fertilizer using biochar as support material. *Science of The Total Environment*, 505:446–453.

[40] Wang, C.; Luo, D.; Zhang, X.; Huang, R.; Cao, Y.; Liu, G.; Zhang, Y.; Wang, H. (2022). Biochar-based slow-release of fertilizers for sustainable agriculture: A mini review. *Environmental Science and Ecotechnology*, 10:100167.

[41] Elkhlifi, Z.; Kamran, M.; Maqbool, A.; El-Naggar, A.; Ifthikar, J.; Parveen, A.; Bashir, S.; Rizwan, M.; Mustafa, A.; Irshad, S.; et al. (2021). Phosphate-lanthanum coated sewage sludge

biochar improved the soil properties and growth of ryegrass in an alkaline soil. *Ecotoxicology and Environmental Safety*, 216: 112173.

[42] Pogorzelski, D.; Filho, J.F.L.; Matias, P.C.; Santos, W.O.; Vergütz, L.; Melo, L.C.A. Biochar as composite of phosphate fertilizer: Characterization and agronomic effectiveness. Science of the Total Environment 2020, 743, 140604, doi:10.1016/j.scitotenv.2020.140604.

[43] Liu, J.; Yang, Y.; Gao, B.; Li, Y.C.; Xie, J. (2019). Bio-based elastic polyurethane for controlled-release urea fertilizer: Fabrication, properties, swelling and nitrogen release characteristics. *Journal of Cleaner Production*, 209:528–537.

[44] Komariah, R.N.; Krishanti, N.P.R.A.; Yoshimura, T.; Umemura, K. (2022). Characterization of Particleboard Using the Inner Part of Oil Palm Trunk (OPT) with a Bio-based Adhesive of Sucrose and Ammonium Dihydrogen Phosphate (ADP). *BioResources*, 17:5190–5206.

[45] Puspita, A.; Pratiwi, G.; Fatimah, I. (2017). Chitosan-modified smectite clay and study on adsorption-desorption of urea. *Chemical Engineering Transactions*, 56:1645–1650.

[46] Sharma, N.; Singh, A.; Dutta, R.K. (2021). Biodegradable fertilizer nanocomposite hydrogel based on poly(vinyl alcohol)/kaolin/diammonium hydrogen phosphate (DAhP) for controlled release of phosphate. *Polymer Bulletin*, 78:2933–2950.

[47] Hussien, R.A.; Donia, A.M.; Atia, A.A.; El-Sedfy, O.F.; El-Hamid, A.R.A.; Rashad, R.T. (2012). Studying some hydro-physical properties of two soils amended with kaolinite-modified cross-linked poly-acrylamides. *CATENA*, 92:172–178.

[48] Rashidzadeh, A.; Olad, A. (2014). Slow-released NPK fertilizer encapsulated by NaAlg-g-poly(AA-co-AAm)/MMT superabsorbent nanocomposite. *Carbohydrate Polymers*, 114:269–278.

[49] Hermida, L.; Agustian, J. (2019). Slow release urea fertilizer synthesized through recrystallization of urea incorporating natural bentonite using various binders. *Environmental Technology & Innovation*, 13:113–121.

[50] Wu, J.; Wei, Y.; Lin, J.; Lin, S. (2003). Study on starch-graft-acrylamide/mineral powder superabsorbent composite. *Polymer*, 44:6513–6520.

[51] Borges, R.; Brunatto, S.F.; Leitão, A.A.; De Carvalho, G.S.G.; Wypych, F. (2015). Solid-state mechanochemical activation of clay minerals and soluble phosphate mixtures to obtain slow-release fertilizers. *Clay Minerals*, 50:153–162.

[52] Mortland, M.M.; Fripiat, J.J.; Chaussidon, J.; Uytterhoeven, J. (1963). Interaction between ammonia and the expanding lattices of montmorillonite and vermiculite. *Journal of Physical Chemistry*, 67:248–258.

[53] Rudmin, M.; Banerjee, S.; Makarov, B.; Belousov, P.; Kurovsky, A.; Ibraeva, K.; Buyakov, A. Glauconite-Urea Nanocomposites As Polyfunctional Controlled-Release Fertilizers. Journal of Soil Science and Plant Nutrition 2022, 22, 4035–4046, doi:10.1007/s42729-022-01006-4.

[54] Rudmin, M.; Banerjee, S.; Yakich, T.; Tabakaev, R.; Ibraeva, K.; Buyakov, A.; Soktoev, B.; Ruban, A. (2020). Formulation of a slow-release fertilizer by mechanical activation of smectite/glauconite and urea mixtures. *Applied Clay Science*, 196:105775.

[55] Hamed, M.; Abdelhafez, A.A. (2020). Application of Glauconite Mineral as Alternative Source of Potassium in Sandy Soils. *Alexandria Science Exchange Journal*, 41:181–189.

[56] Karimi, E.; Abdolzadeh, A.; Sadeghipour, H.R.; Aminei, A. (2012). The potential of glauconitic sandstone as a potassium fertilizer for olive plants. *Archives of Agronomy and Soil Science*, 58:983–993.

[57] Oze, C.; Smaill, J.B.; Reid, C.M.; Palin, M. (2019). Potassium and Metal Release Related to Glaucony Dissolution in Soils. *Soil Systems*, 3:1–17.

[58] Drits, V.A.; Zviagina, B.B.; McCarty, D.K.; Salyn, A.L. (2010). Factors responsible for crystal-chemical variations in the solid solutions from illite to aluminoceladonite and from glauconite to celadonite. *American Mineralogist*, 95:348–361.

[59] Drits, V.A. (1997). Isomorphous Cation Distribution in Celadonites, Glauconites and Fe-illites Determined by Infrared, Mössbauer and EXAFS Spectroscopies. *Clay Minerals*, 32:153–179.

[60] Odin, G.S.; Matter, A. (1981). De glauconiarum origine. *Sedimentology*, 28:611–641.

[61] Odom, I.E. (1984). 13. GLAUCONITE and CELADONITE MINERALS. *In Micas; Bailey,*

S.W., Ed.; De Gruyter; pp. 545–572.

[62] Rieder, M.; Cavazzini, G.; D'yakonov, Y.S.; Frank-Kamenetskii, V.A.; Gottardi, G.; Guggenheim, S.; Koval', P.V.; Müller, G.; Neiva, A.M.R.; Radoslovich, E.W.; et al. (1988). Nomenclature of the micas. *Canadian Mineralogist*, 36:905–912.

[63] McRae, S.G. (1972). Glauconite. *Earth-Science Reviews*, 8:397–440.

[64] Basak, B.B.; Sarkar, B.; Maity, A.; Chari, M.S.; Banerjee, A.; Biswas, D.R. (2023). Low-grade silicate minerals as value-added natural potash fertilizer in deeply weathered tropical soil. *Geoderma*, 433:116433.

[65] Rudmin, M.; Banerjee, S.; Makarov, B. (2020). Evaluation of the Effects of the Application of Glauconitic Fertilizer on Oat Development: A Two-Year Field-Based Investigation. *Agronomy*, 10:872.

[66] Zviagina, B.B.; Drits, V.A.; Sakharov, B.A.; Ivanovskaya, T.A.; Dorzhieva, O. V.; McCarty, D.K. (2017). Crystal-chemical regularities and identification criteria in Fe-bearing k-dioctahedral micas 1m from X-Ray diffraction and infrared spectroscopy data. *Clays and Clay Minerals*, 65:234–251.

[67] López-Quirós, A.; Sánchez-Navas, A.; Nieto, F.; Escutia, C. (2020). New insights into the nature of glauconite. *American Mineralogist*, 105:674–686.

[68] Amorosi, A.; Sammartino, I.; Tateo, F. (2007). Evolution patterns of glaucony maturity: A mineralogical and geochemical approach. *Deep Sea Research Part II: Topical Studies in Oceanography*, 54:1364–1374.

[69] Rudmin, M.; López-Quirós, A.; Banerjee, S.; Ruban, A.; Shaldybin, M.; Bernatonis, P.; Singh, P.; Dauletova, A.; Maximov, P. (2023). Origin of Fe-rich clay minerals in Early Devonian volcanic rocks of the Northern Minusa basin, Eastern Siberia. *Applied Clay Science*, 241:107014.

[70] Rudmin, M.; Banerjee, S.; Makarov, B.; Mazurov, A.; Ruban, A.; Oskina, Y.; Tolkachev, O.; Buyakov, A.; Shaldybin, M. (2019). An investigation of plant growth by the addition of glauconitic fertilizer. *Applied Clay Science*, 180:1–8.